

Article

On the Innovation, Design, Construction, and Experiments of OMEGA-Based SSPS Prototype: The Sun Chasing Project

Baoyan Duan, Yiqun Zhang, Guangda Chen, Ze Zhao, Jianwei Mi, Xun Li,  
Lin Yang, Xi Li

PII: S2095-8099(23)00473-3

DOI: <https://doi.org/10.1016/j.eng.2023.11.007>

Reference: ENG 1408

To appear in: *Engineering*

Received Date: 6 December 2022

Revised Date: 24 February 2023

Accepted Date: 27 November 2023

Please cite this article as: B. Duan, Y. Zhang, G. Chen, Z. Zhao, J. Mi, X. Li, L. Yang, X. Li, On the Innovation, Design, Construction, and Experiments of OMEGA-Based SSPS Prototype: The Sun Chasing Project, *Engineering* (2023), doi: <https://doi.org/10.1016/j.eng.2023.11.007>

This is a PDF file of an article that has undergone enhancements after acceptance, such as the addition of a cover page and metadata, and formatting for readability, but it is not yet the definitive version of record. This version will undergo additional copyediting, typesetting and review before it is published in its final form, but we are providing this version to give early visibility of the article. Please note that, during the production process, errors may be discovered which could affect the content, and all legal disclaimers that apply to the journal pertain.

## Research

Microwave Wireless Power Transfer Technology–Article

# **On the Innovation, Design, Construction, and Experiments of OMEGA-Based SSPS Prototype: The Sun Chasing Project**

Baoyan Duan <sup>a,\*</sup>, Yiqun Zhang <sup>a</sup>, Guangda Chen <sup>a</sup>, Ze Zhao <sup>a</sup>, Jianwei Mi <sup>a</sup>, Xun Li <sup>a</sup>, Lin Yang <sup>b</sup>, Xi Li <sup>b</sup>

<sup>a</sup> Research Institute on Mechatronics, Xidian University, Xi'an 710071, China

<sup>b</sup> Research Institute of Antenna, Xidian University, Xi'an 710071, China

\* Corresponding author.  
E-mail address: byduan@xidian.edu.cn (B. Duan).

## **ARTICLE INFO**

*Article history:*

Received 6 December 2022

Revised 24 February 2023

Accepted 27 November 2023

Available online

*Keywords:*

OMEGA-SSPS

Full-link and full-system

Beam collection efficiency

Circular stepped beam shape

Smart structure

Field coupling theoretical model

Beam pointing control

## **ABSTRACT**

This study systematically introduces the development of the world's first full-link and full-system ground demonstration and verification system for the OMEGA space solar power satellite (SSPS). First, the OMEGA 2.0 innovation design was proposed. Second, field-coupling theoretical models of sunlight concentration, photoelectric conversion, and transmitting antennas were established, and a systematic optimization design method was proposed. Third, a beam waveform optimization methodology considering

both a high beam collection efficiency and a circular stepped beam shape was proposed. Fourth, a control strategy was developed to control the condenser pointing toward the sun while maintaining the transmitting antenna toward the rectenna. Fifth, a high-efficiency heat radiator design method based on bionics and topology optimization was proposed. Sixth, a method for improving the rectenna array's reception, rectification, and direct current (DC) power synthesis efficiencies is presented. Seventh, high-precision measurement technology for high-accuracy beam-pointing control was developed. Eighth, a smart mechanical structure was designed and developed. Finally, the developed SSPS ground demonstration and verification system has the capacity for sun tracking, a high concentration ratio, photoelectric conversion, microwave conversion and emission, microwave reception, and rectification, and thus satisfactory results were obtained.

## 1 Introduction

The development and utilization of solar energy are extremely favorable options because of the limited amount of coal and fossil energy available for exploitation [1], the increasing challenges posed by climate change on Earth, and China's carbon peak and carbon neutralization targets. The solar power density on the ground is approximately  $136 \text{ W} \cdot \text{m}^{-2}$ , whereas in space, this value can be as high as  $1360 \text{ W} \cdot \text{m}^{-2}$ . If a space condenser were adopted, the concentrated solar power density would be very noticeable.

Space solar power satellites (SSPS) have various future applications. Although it is difficult to supply power from outer space to the ground in the short term, it has many other applications, such as building charging piles in a synchronous solar orbit to charge many small satellites. This space infrastructure can address the power supply problems of small satellites operating in low or medium orbits. Therefore, the construction of the SSPS is crucial.

It has been 54 years since Peter Glaser first proposed the SSPS concept in 1968 [2]. Over the past 50 years, SSPS research has had its highs and lows. However, SSPS research has not ceased. Research activities on SSPS have mainly focused on innovative concept designs and experimental validations.

Innovative SSPS concepts can be divided into two categories: non-concentrating and concentrating. The representative concepts of non-concentrating SSPS include the 1979 SSPS reference model [3], European sail tower SSPS [4], tethered-SSPS [5], and multi-rotary joint SSPS [6]. The representative concepts of concentrating SSPS include the integrated symmetrical concentrator SSPS [7], ALPHA-SSPS [8], stepped module concept utilized to relieve the heat dissipation problems of the sandwich concept [9], and OMEGA [10–12]. In addition, some hybrid concepts include both concentrating and non-concentrating, such as the CASSIOPeia SSPS [13] and tile SSPS [14].

Note that the verification experiments conducted thus far only focus on one aspect of the SSPS; one can hardly find a complete microwave wireless power transmission

(MWPT) experiment. In 2008, National Aeronautics and Space Administration (NASA) conducted an MWPT experiment with the longest transmission distance (148 km) between Mauna Loa Island and Haleakala Island in Hawaii [15]. An active phased-array antenna was utilized as the transmitting antenna, and solid-state power amplifiers were employed. The working frequency of the transmitting frequency was 2.45 GHz, and 20 W of power was transmitted. This experiment preliminarily validated the feasibility of the MPWT over large distances. However, this study has two limitations. First, the efficiency of microwave transmission is extremely low. Second, the MWPT subsystem of an SSPS was validated in the experiment, and the solar energy collection and conversion subsystem was not included, which means that the experimental validation was not completed.

In 2015, an MWPT experiment was conducted in the Hyogo Prefecture, Japan [16]. The transmission distance was 55 m. The experiment validated the power transmission based on a phased array with 5.8 GHz solid-state power amplifiers. The transmission power was 1.8 kW, and the DC–DC transmission efficiency was 9.88%. The Japanese experiment was a big step ahead of the USA experiment. However, this study had some limitations. Specifically, it only validated DC to radio frequency 1 (RF1) conversion, microwave power transmission (RF1 to RF2), and microwave power reception and conversion (RF2–DC). In addition, it could not simulate links such as sun tracking, high concentration ratios, photoelectric conversion, and DC power management of an SSPS in orbit.

In addition, an experiment was conducted in 2019 employing a phased array to power a flying drone. For the flying drone, DC power of approximately 60 W was received at a distance of 10 m. When the distance was increased to 30 m, the received DC power was approximately 42 W [17].

In 2020, the US Navy Research Laboratory (NRL) launched a sandwich module aboard the Air Force X-37B orbital test vehicle [18]. The sandwich module was a 12 inch (1 inch = 2.54 cm) square tile that collects solar energy and converts it into RF power. In the same year, the US NRL utilized a light-emitting rectenna to convert wireless network signals into DC power. The experiment was conducted at the International Space Station [19].

Meaningful research has been conducted for experimental verification in China. In 2009, Professor Kama Huang's research group at Sichuan University [20] developed a ground-based MWPT system with the phase-locked magnetron technology. The transmitting antenna had an aperture size of 1.5 m × 2.4 m, while the rectenna had an aperture size of 2.7 m × 8.0 m. In the MWPT experiment, the transmission distance was 200 m, the working frequency was 2.45 GHz, the beam collection efficiency was 55%, and the transmission efficiency from RF to DC was 2.25%.

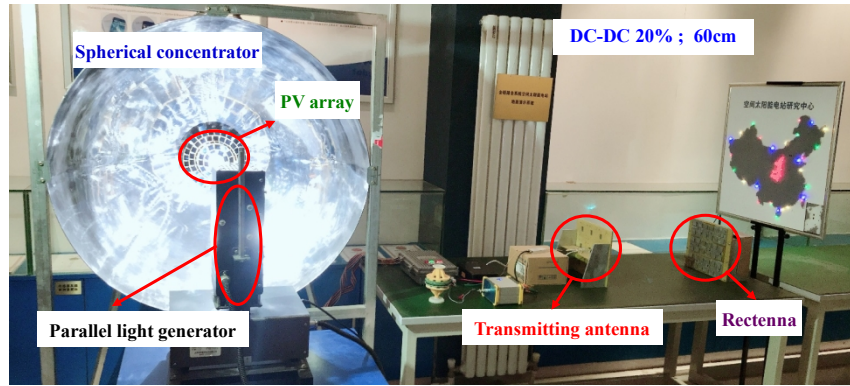
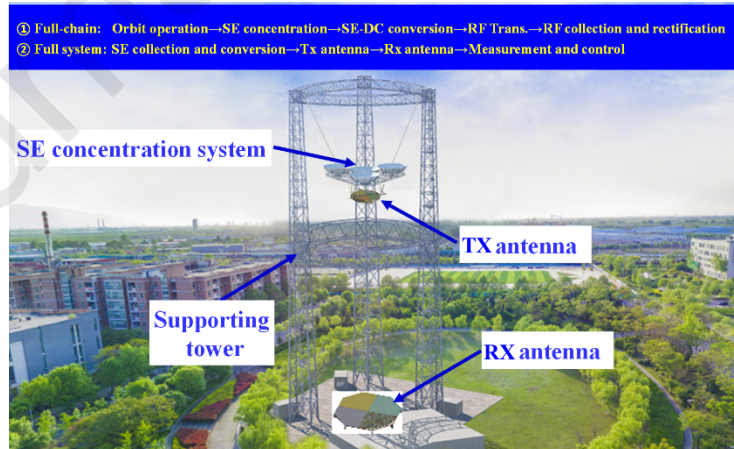


**Fig. 1.** OMEGA demonstration verification device located indoors. PV: photovoltaic.

Apart from Sichuan University, Xidian University developed a full-link, full-system indoor experimental system (presented in Fig. 1). The system included a parallel light generator to mimic incoming sunlight, a hemispherical condenser, a photoelectric conversion system, microwave conversion and emission, and a microwave rectenna. A solid-state power amplifier was utilized to drive a subarray with four air-substrate microstrip patch elements for the transmitting antenna. The rectenna had nine air-substrate microstrip patch elements. Both the power amplifier and rectifier circuits exhibited efficiencies of approximately 50%. However, the system had two defects: an indoor system and a short transmission distance (60 cm).

To investigate key technologies such as microwave beaming, sun tracking of the condenser, high concentration ratio and photoelectric conversion, RF power conversion, and transmitting antenna, RF power collection and rectification, smart design of the space structural system, precision measurement, and overall system control, an outdoor SSPS ground demonstration and verification system was constructed at Xidian University (Fig. 2).



(a)

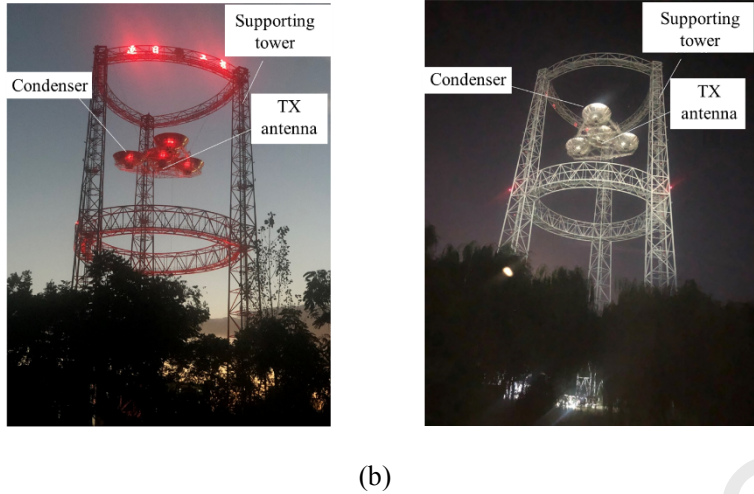


**Fig. 2.** (a) Outdoor OMEGA-SSPS ground demonstration and verification system, and (b) prototype of OMEGA-SSPS ground demonstration and verification system. SE: sun energy; TX: transmission antenna; RX: receiving antenna.

## 2 Innovation of OMEGA 2.0

Two issues exist with the OMEGA-SSPS concept proposed in 2014 [10–12]. First, the concept requires a special type of thin-film material to be utilized as a spherical condenser. Second, a high-voltage, high-power DC conductive slip ring is required. To overcome these issues, an improved design concept, OMEGA 2.0 [21,22] was proposed by our research group, as illustrated in Fig. 3. In OMEGA 2.0, a hemispherical condenser is utilized to replace the entire spherical condenser, and two transmitting antennas are placed outside the condenser. It should be stressed that the number of transmitting antennas can vary based on practical requirements. For example, only one transmitting antenna is adopted in a ground verification system. This novel design concept overcomes two major issues in the original design. An electronically scanned array with vertical dipoles can maintain the transmitted beam pointing toward the rectenna. In addition, to realize the objective of the condenser pointing toward the sun in real time, the position and attitude of the condenser should be adjusted. Therefore, electric propulsion technology was adopted.

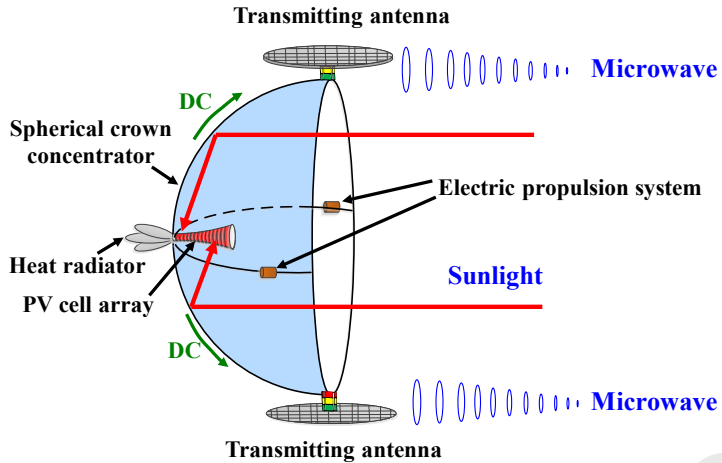


**Fig.3.** OMEGA 2.0 innovative design concept.

### 3 Coupling model of multiple physical systems and design theory model

The space segment of the OMEGA 2.0 system comprises three subsystems: the hemispherical condenser and photoelectric conversion, transmitting antenna and microwave conversion, and a smart-structure subsystem with a high-power mass ratio. This complicated system involves several problems, such as the coupling problem of the electromagnetic field, temperature field, structural displacement field, and other physical fields; the influence mechanism of nonlinear mechanical, structural, and material factors on electrical and optical performance; and the systematic optimization design problem based on the developed multifield coupling theory model and influence mechanism [23]. The optimization design problem can be mathematically described as a nonlinear programming problem PI, that is, determining the optimum structure and thermal and electromagnetic design variables to maximize the system power mass ratio [23]. For the optimization model, several constraints exist, such as electromagnetic, structural, and thermal performance constraints, the coupling theoretical model and influence mechanism constraint, and the manufacturing and size constraint, and so on.

$$\begin{aligned} \text{Find } & \quad \mathbf{X} = (x_1, x_2, \dots, x_{nud})^T \\ \min & \quad -Z(\mathbf{X}) \end{aligned} \tag{1a}$$

$$\text{s. t. } g_j^S(\mathbf{X}) \leq 0, \quad j = 1, 2, \dots, \text{NUS} \tag{1b}$$

$$g_j^T(\mathbf{X}) \leq 0, \quad j = 1, 2, \dots, \text{NUT} \tag{1c}$$

$$g_j^E(\mathbf{X}) \leq 0, \quad j = 1, 2, \dots, \text{NUE} \tag{1d}$$

$$g_j^C(\mathbf{X}) \leq 0, \quad j = 1, 2, \dots, \text{NUC} \tag{1e}$$

$$\Gamma_1(S_N, \delta(\beta), \gamma, T, F) = 0 \tag{1f}$$

$$\Gamma_2(E_{\text{op}}, T, \delta(\beta), \gamma, F) = 0 \quad (1g)$$

$$\Gamma_3(E, T, \delta(\beta), \gamma, F) = 0 \quad (1h)$$

$$\bar{f}(M^i, V^i, J^i, L^i, x, y, z | i=1, 2, 3) = 0 \quad (1i)$$

$$\underline{X} \leq X \leq \bar{X} \quad (1l)$$

where  $X$  is design variable vector,  $x_{\text{nud}}$  is the total number of design variables,  $Z$  is the power mass ratio, and  $\bar{f}$  is the compatibility constraint.  $g^S, g^T, g^E$ , and  $g^C$  are the constraints for struture, temperature, electronic, and control aspects, respectively.  $\Gamma_1, \Gamma_2$ , and  $\Gamma_3$  stand for three subsystems, that is, optical condenser, photovoltaic (PV), and transmission antenna, respectively.  $x, y$ , and  $z$  are the coordinates of mass center of three subsystems. NUS, NUT, NUE, and NUC are the total number of nonlinear constraint functions of the structure, thermal, electromagnetic, and control, respectively.

Eq. (1a) represents the objective of maximizing the system power-to-mass ratio. Eqs. (1b)–(1e) present the performance constraints of the structure, thermal conversion, photoelectric conversion, and control subsystems, respectively. Eqs. (1f)–(1h) represent the field-coupling theoretical models of the sunlight concentration, photoelectric conversion, and transmitting antennas, respectively. The influence mechanism was included in the field-coupling models. Equation 1i is the required compatibility equation ( $i=1, 2, 3$ ) of mass  $M^i$ , inertia  $J^i$ , volume  $V^i$ , and characteristic dimension  $L^i$  of the sunlight concentration, photoelectric conversion, and transmission antenna subsystems. Eq. (1l) represents the upper and lower bound constraints of design variables. Parameters  $S_N, \delta(\beta), \gamma, T, F, E$ , and  $E_{\text{op}}$  represent the light pressure, displacement (structural parameter), random error caused by manufacturing and assembly, temperature, control force, and electromagnetic and solar power density distribution of the PV array, respectively.

Utilizing the coupling model and design theory, the aerial structure of the ground verification system, illustrated in Fig. 4, was designed. The structure had four hemispherical condensers, a top-shaped PV array, a supporting frame, and a power management and distribution (PMAD) system. To adapt to the traction and driving requirements of the three cables (utilizing three cables, the entire structure presented in Fig.4 was lifted to a height of 55 m, and the rectenna was placed on the ground), the four condensers were arranged in a triangle.

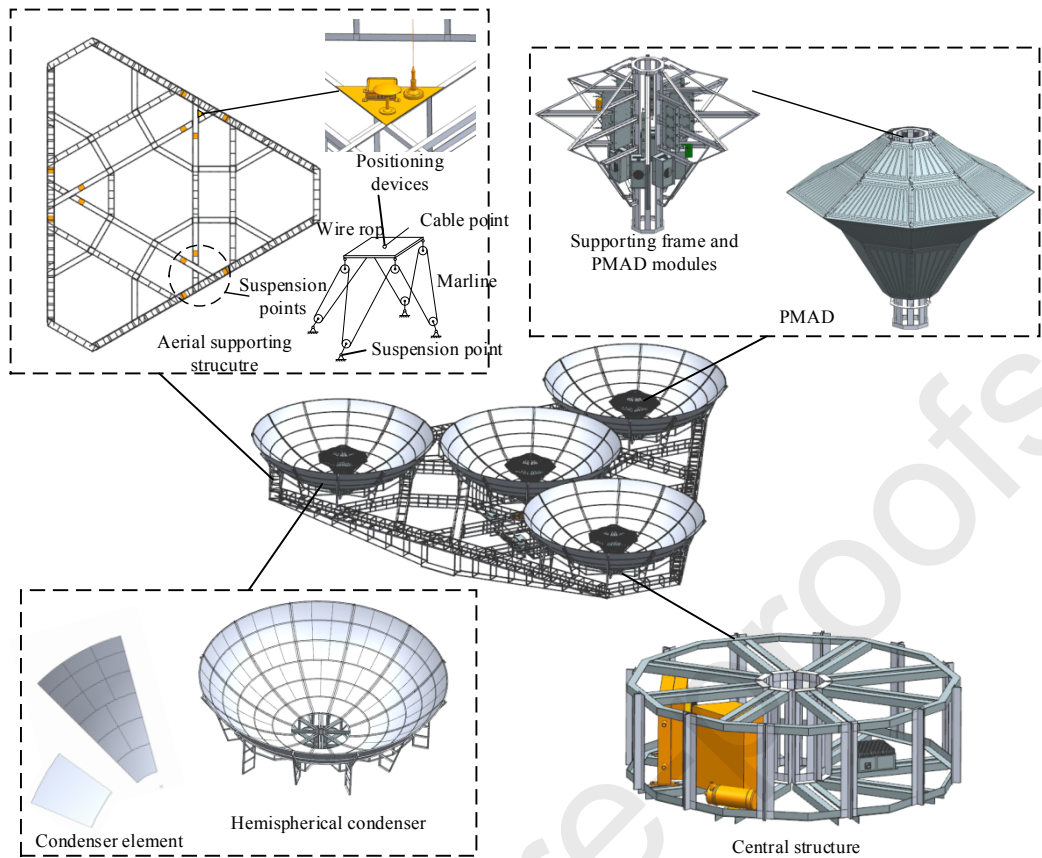


**Fig. 4.** Aerial structure of ground verification system. PMAD: power management and distribution.

To ensure the surface accuracy of the PV panel, a PV array supporting frame was designed, as illustrated in Fig. 5, where an aluminum channel was employed to form the backbone structure. The designed structure can also provide sufficient space for the PMAD modules and is connected to the central structure, as depicted in Fig. 5. The central structure consists of two heat radiators, a water tank, a water pump, and a temperature measurement module, and is fixed with a supporting frame.

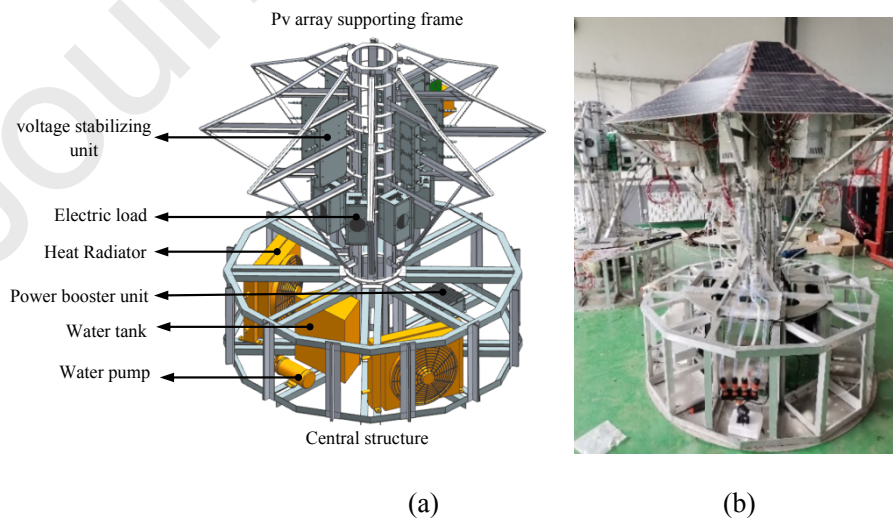


**Fig. 5.** Three-dimensional (3D) model and prototype of central structure, supporting frame, and top-

shaped PV array: (a) 3D model and (b) prototype.

A finite element model (FEM) was established based on the three-dimensional (3D) model of the aerial structure presented in Fig. 4, as illustrated in Fig. 6. The supporting frame was simulated with a beam element, condenser panel was simulated with a shell element, and the PV array panel was simulated with a plate element. A gravitational load was applied to the model to analyze its structural performance. In addition, the loads posed by the PMAD, measurement and control, and heat dissipation modules were treated as the loads. In the FEM, they are placed in associated nodes. The ambient temperature load is applied in accordance with 35 °C. Considering the adverse meteorological conditions (rain, snow, strong wind, etc.), the experiment was not conducted; therefore, only the steady-state wind load was considered, as illustrated in Fig. 7.

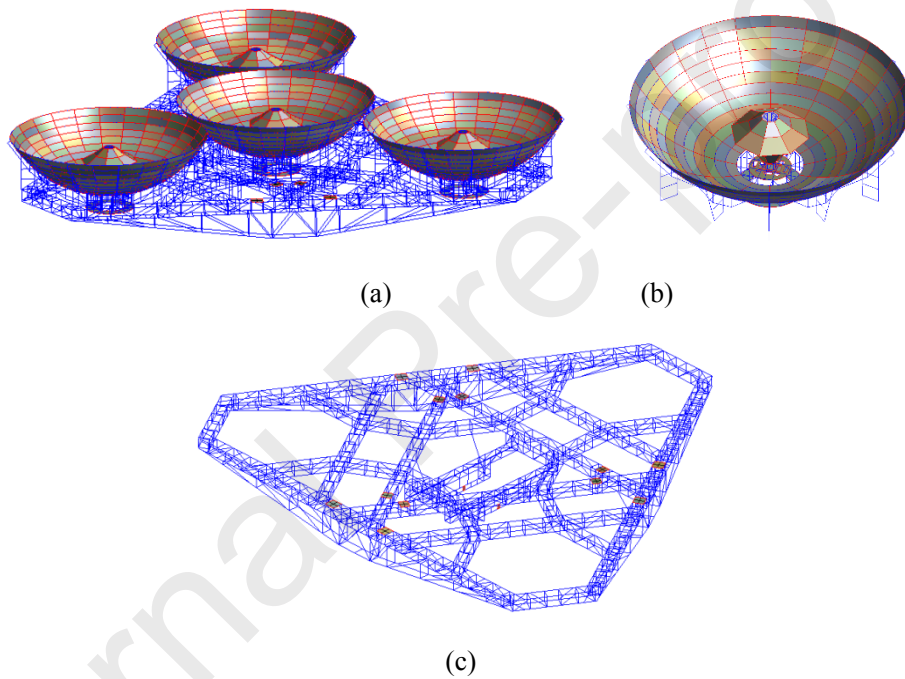


**Fig. 6.** FEM of aerial structure. (a) Overall structure; (b) condenser PV array structure; (c) supporting information.

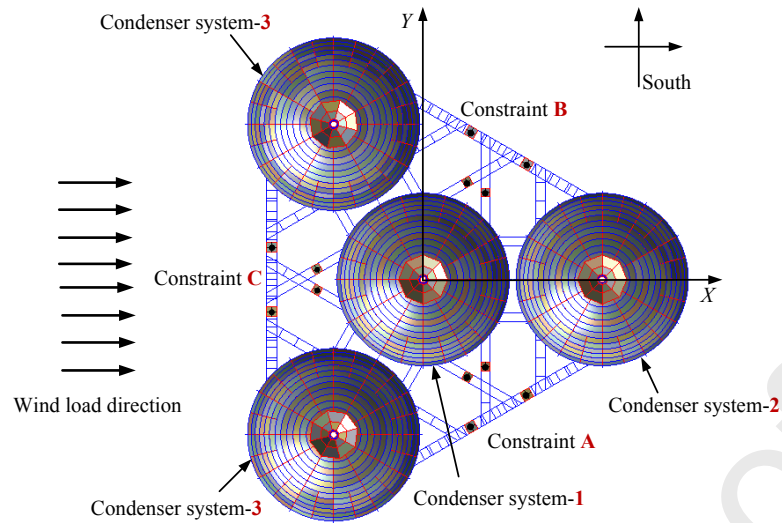


**Fig. 7.** Load and constraint of FEM model of aerial structure. A, B, and C: the three suspension points.

The structural performance was analyzed with the established FEM model. Subsequently, its performance was optimized based on the coupling model of multiple physical systems and design theory. The objective was to maximize the power-to-mass ratio of the aerial system. To simulate an SSPS operating in outer space, the ground verification system should be able to track the sun. Thus, in the optimization process, two conditions were considered. The first is when the entire structure is in a horizontal working condition, and the second is when a given angle tilts the entire structure. According to the latitude where the ground verification system is located, the maximum north-south tilt angle of the aerial structure is approximately 58°. The structural deformation and stress nephograms for the horizontal working conditions are presented in Fig. 8. The performance of the entire structure under the worst-inclined working condition (tilted angle = 58°) was also analyzed, and the structural deformation and stress nephogram are plotted in Fig. 9.

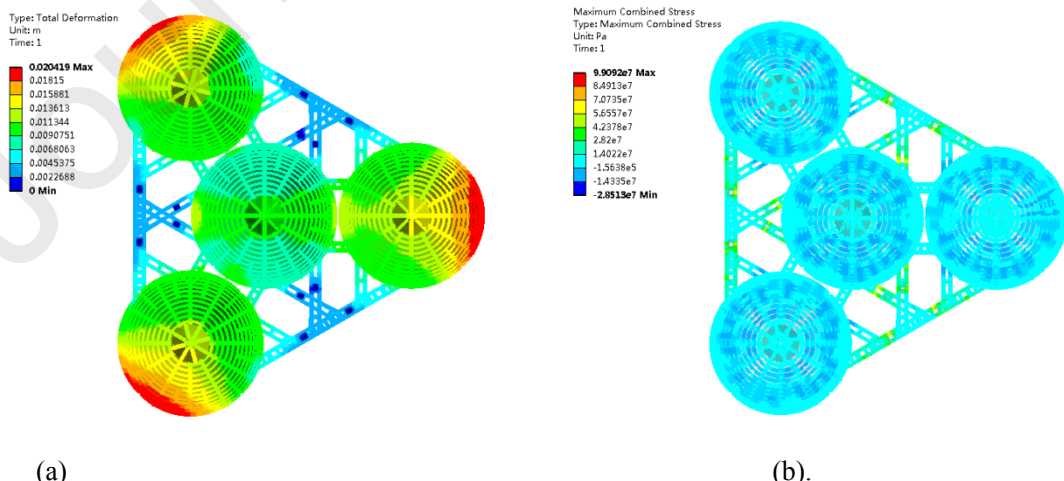
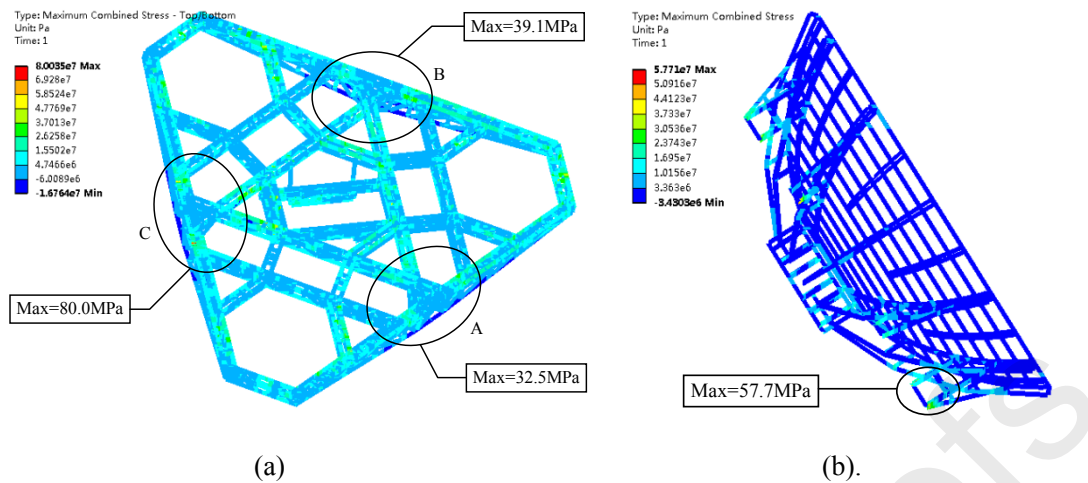


Fig. 8 (a) Deformation nephogram, and (b) stress nephogram of entire structure in horizontal working condition.



**Fig. 9.** (a) Deformation nephogram, and (b) stress nephogram of entire structure in inclined working condition (tilted angle = 58 °).

Table 1 summarizes the maximum stresses of the key parts of the aerial structure at different tilt angles. Generally, as the tilted angle increases, the stress of each key part of the aerial structure increases.

**Table 1**

Maximum stress of key parts of aerial structure at different tilted angles.

Tilt angle (°)	Maximum stress (MPa)									
	Suspension structure			overall PV array structure			supporting condenser structure			supporting
	A	B	C	1	2	3	1	2	3	
10	64.0	59.8	72.9	34.5	35.7	36.3	22.0	22.5	23.4	
20	62.1	50.7	71.5	48.1	49.4	49.9	23.9	24.7	25.0	
30	56.8	45.8	66.4	60.2	61.9	62.5	32.9	33.8	34.5	
40	48.3	43.8	63.2	70.3	72.1	72.5	43.2	44.1	45.1	
50	37.2	41.7	74.9	78.5	79.7	79.9	51.6	52.8	53.3	

1, 2, and 3 represent the three condenser systems.

#### 4 Microwave transmitting antenna and waveform optimization

The voltage of the DC power obtained from photoelectric conversion is first boosted, then transmitted, and reduced to meet the voltage requirement of power amplifiers. Finally, the DC power is converted to RF power. The converted RF power was transmitted through power amplifiers, power dividers, and radiation elements. The RF power was coherently added and transmitted to the receiving antenna wirelessly. The RF beam waveform is important. The basic requirement for a transmitting antenna is a high beam collection efficiency (BCE), which means that the transmitted power should be concentrated within the main beam as much as possible. The receiving antenna size is determined by the size of the transmitting antenna, distance between the transmitting antenna and rectenna, working frequency, and required BCE. The sidelobe level (SLL) must be as low as possible to enhance the achievable BCE and avoid interference with nearby communication/radar systems. In addition, the power density distribution on the rectenna plane should have a circular stepped shape, as illustrated in Fig. 10(a), which is significantly different from the beam shape adopted for radar or communication, as illustrated in Fig. 10(b). With this beam shape, the power density in each ring is the same. Then, the microwave rectifier circuits utilized in each ring are the same, which meets the high-cost requirements [24].

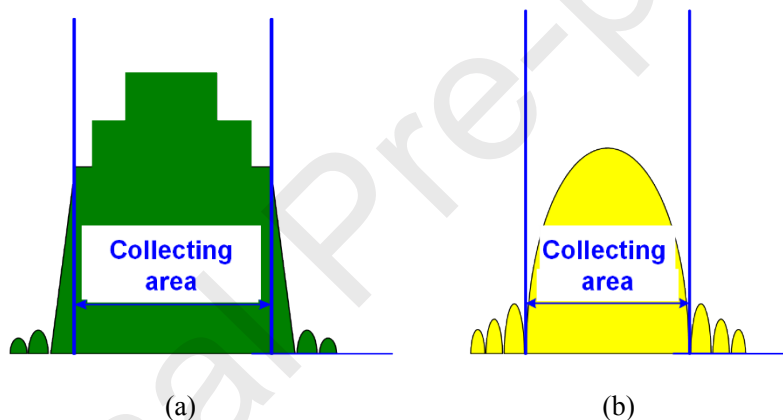


**Fig. 10.** Microwave beam shapes for different applications: (a) for microwave power transmission and (b) for radar or telecommunication.

In addition, the receiving antenna must be located in the far-field zone of the transmitting antenna. This is because the microwave power cannot be radiated in the near field. To address security concerns, the peak microwave power density outside the receiving antenna should be lower than the value specified in national standards.

It is necessary to optimize the amplitude and position of the antenna elements to meet these requirements.

#### 4.1 Stepped amplitude distribution

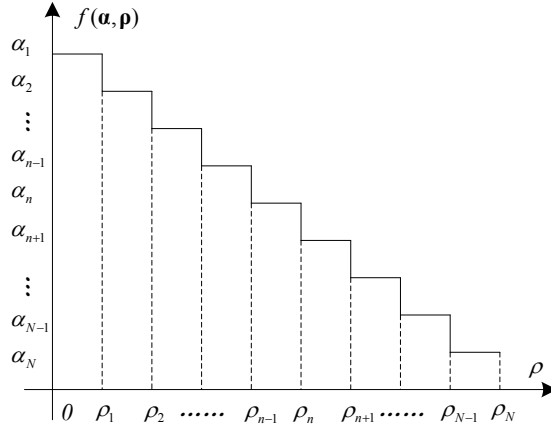


Fig. 11. Illustration of stepped amplitude distribution.

We assume that the normalized stepped amplitude distribution (SAD) is circularly symmetrical and has  $N$  steps, as illustrated in Fig. 11. For the transmitting array antenna, this means that the radiating elements located in each step have the same excitation amplitude. The excitation coefficients differ for elements located in different steps. The Heaviside step function can be described as  $f(\alpha, \rho)$ .

$$f(\alpha, \rho) = \begin{cases} \alpha_1 H(\rho) - \sum_{n=1}^{N-1} (\alpha_n - \alpha_{n+1}) H(\rho - \rho_n) & 0 \leq \rho \leq 1 \\ 0 & \rho > 1 \end{cases} \quad (2a)$$

where  $H(\rho)$  denotes the Heaviside step function.  $\alpha_n$  and  $\rho_n$  are the normalized “height” and “radius” of the  $n$ th ( $n = 1, 2, \dots, N$ ) step of the SAD, respectively; and  $N$  represents the total number of steps. Fig. 11 gives a pictorial explanation of  $\alpha_n$ ,  $\rho_n$ , and  $N$ . To describe the SAD more accurately, the value of the Heaviside step function at point zero is changed from 0.5 to 1, that is

$$H(\rho) = \begin{cases} 1 & \rho \geq 0 \\ 0 & \rho < 0 \end{cases} \quad (2b)$$

The aperture field distribution of the transmitting antenna determines the BCE of an MWPT system. For the proposed SAD distribution, the BCE is related to the number of steps  $N$ , normalized height  $\alpha_n$ , and radius  $\rho_n$  for each step.

#### 4.2 Microwave beam waveform optimization

Waveform optimization can then be summarized as seeking an optimal set of normalized step height  $\alpha_n$  and radii  $\rho_n$  to maximize the achievable BCE, that is,

$$\begin{aligned} \text{Find } X &= (\alpha_1, \alpha_2, \dots, \alpha_N, \rho_1, \rho_2, \dots, \rho_N)^T \\ \min f(X) &= -\text{BCE}(X) \end{aligned} \quad (2c)$$

$$\text{s. t. } g_1(X) \leq C_0 \quad (2d)$$

$$g_2(X) \leq C_1 \quad (2e)$$

$$\alpha_{n+1} \leq \alpha_n, \quad (1 \leq n \leq N-1) \quad (2f)$$

$$\rho_{n+1} \geq \rho_n \quad (1 \leq n \leq N-1) \quad (2g)$$

$$0 < \alpha_n, \rho_n \leq 1, \quad (n=1,2,\dots,N) \quad (2h)$$

where design variable  $X = (\alpha_1, \alpha_2, \dots, \alpha_N, \rho_1, \rho_2, \dots, \rho_N)^T$  denotes the shape description parameters of the SAD, as illustrated in Fig.11. Objective function  $f(X)$  equals  $-\text{BCE}(X)$ , and a negative sign is utilized to make it a standard minimization problem, where  $g_1(X)$  and  $g_2(X)$  are the peak microwave power densities within and outside the rectenna, respectively, and  $C_0$  and  $C_1$  are the corresponding maximum allowable values. The constraint in Eq. (2f) is utilized to ensure that the amplitude of the SAD decreases from the center to the edge to decrease the SLL, similar to other amplitude tapers. The constraint in Eq. (2g) is utilized to make the “width” of each step larger than zero.

In the project, the transmitting antenna and rectenna had circular apertures with diameters of 1.2 and 5.2 m, respectively. A distance of 55 m separated them. Fig. 12 presents the optimized layout of the four-step SAD distribution utilized in the ground demonstration system. The transmitting antenna contains 176 subarrays and four types of power amplifiers. A schematic of the transmitting antenna is presented in Fig. 13. It mainly comprises a 5.8 GHz crystal oscillator, a 1-to-176 power divider, 176 power amplifier channels, and 176 transmitting subarrays. Each power amplifier channel has a power amplifier and a phase shifter. The DC power comes from solar energy collection, and the conversion subsystem feeds the transmitting antenna subsystem.

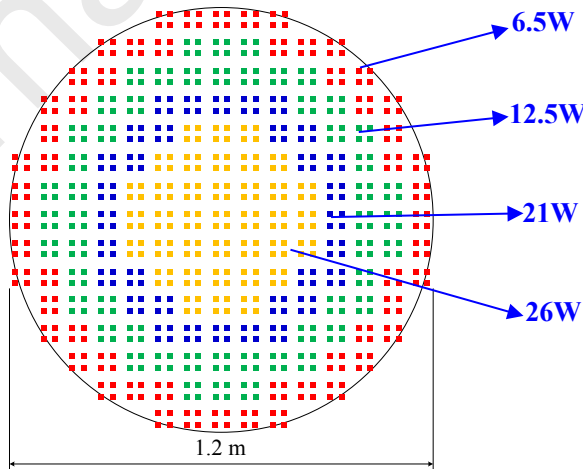


**Fig. 12.** Power amplifier layout of transmitting antenna.

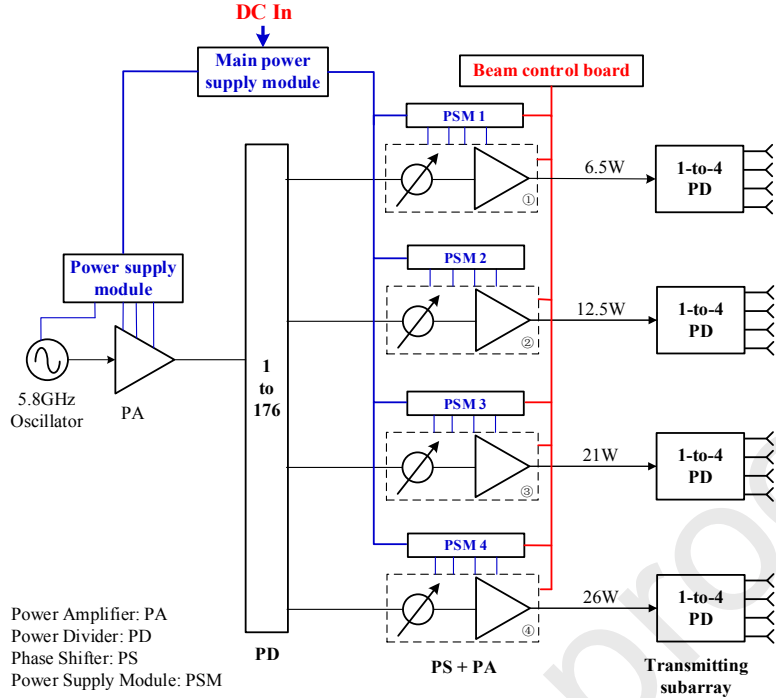


**Fig. 13.** Schematic of transmitting antenna. PA: power amplifier; PD: power divider; PS: phase shifter; PSM: power supply module.

## 5 Orientation control of condenser to sun and transmitting antenna to receiving antenna

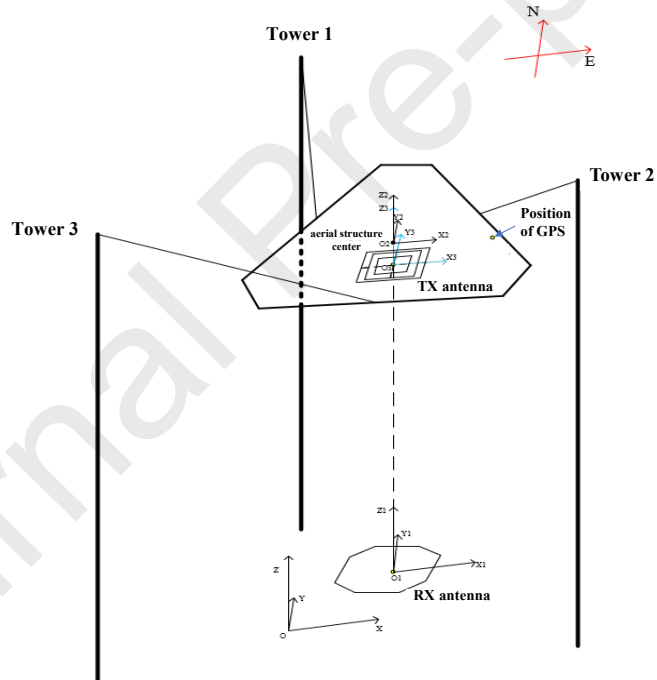
First, the coordinate system of the ground verification system presented in Fig. 14(a) is established, and it is specified that  $X$ ,  $Y$ , and  $Z$  point to the east, north, and sky respectively. In Fig. 14(a),  $OXYZ$  is the geodetic coordinate system,  $O_1X_1Y_1Z_1$  indicates the receiving antenna coordinate system,  $O_2X_2Y_2Z_2$  refers to the overall aerial structure coordinate system, and  $O_3X_3Y_3Z_3$  denotes the transmitting antenna coordinate system. To realize the objective of condenser tracking to the sun in real time, the entire aerial structure is suspended with three long-span flexible cables through a 75 m high support tower. In addition, by adjusting the length of three cables, requirements on the altitude, position, and attitude of the aerial structure and condenser can be met. The detailed aerial structure is presented in Fig. 14(b), which includes four hemispherical condensers and the top-shaped PV array, supporting frame, transmitting antenna, and the power management and distribution system. There are three Beidou position and attitude sensors, which can give the position coordinate of the aerial structure center  $(x_{c1}, y_{c1}, z_{c1})^T$  and attitude angle ( $\bar{\alpha}$  and  $\bar{\beta}$ ) in real time. In addition, the ground position coordinate  $(x_{c0}, y_{c0}, z_{c0})^T$  can also be given. Then, the position coordinate of the aerial structure in the ground coordinate  $OXYZ$ , i.e.,  $(x_{wl}, y_{wl}, z_{wl})^T$  and yaw angle ( $\bar{\gamma}$ ) can be calculated by

$$\begin{bmatrix} x_{w1} \\ y_{w1} \\ z_{w1} \end{bmatrix} = \mathbf{R}(\bar{\alpha}, \bar{\beta}, \bar{\gamma}) \cdot \begin{bmatrix} x_{c1} \\ y_{c1} \\ z_{c1} \end{bmatrix} + \begin{bmatrix} x_{c0} \\ y_{c0} \\ z_{c0} \end{bmatrix} \quad (3a)$$

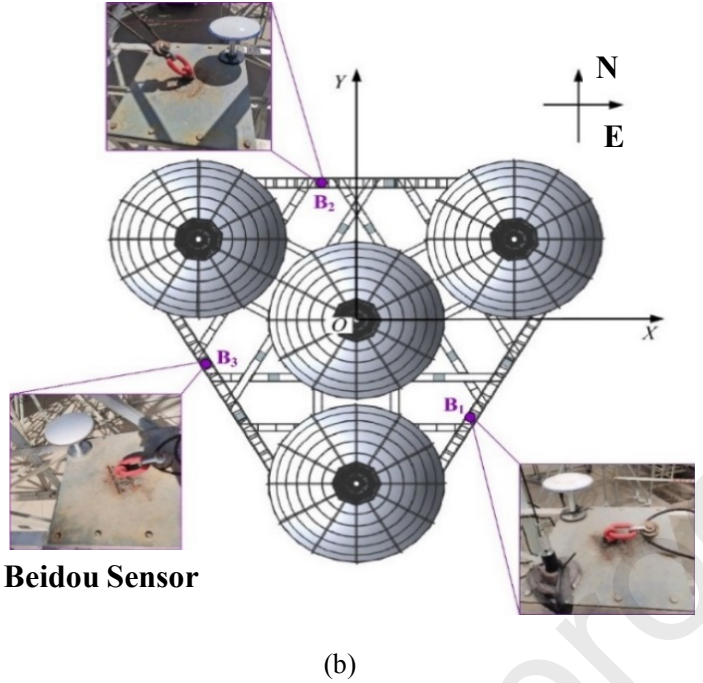
$$\begin{bmatrix} \tilde{x}_{c1} \\ \tilde{y}_{c1} \\ \tilde{z}_{c1} \end{bmatrix} = \begin{bmatrix} \cos \bar{\beta} \cos \bar{\gamma} - \sin \bar{\alpha} \sin \bar{\beta} \sin \bar{\gamma} & -\cos \bar{\alpha} \sin \bar{\gamma} & \sin \bar{\beta} \cos \bar{\gamma} + \sin \bar{\alpha} \cos \bar{\beta} \sin \bar{\gamma} \\ \cos \bar{\beta} \sin \bar{\gamma} + \sin \bar{\alpha} \sin \bar{\beta} \cos \bar{\gamma} & \cos \bar{\alpha} \cos \bar{\gamma} & \sin \bar{\beta} \sin \bar{\gamma} - \sin \bar{\alpha} \cos \bar{\beta} \cos \bar{\gamma} \\ -\cos \bar{\alpha} \sin \bar{\beta} & \sin \bar{\alpha} & \cos \bar{\alpha} \cos \bar{\beta} \end{bmatrix} \begin{bmatrix} x_{c1} \\ y_{c1} \\ z_{c1} \end{bmatrix} \quad (3b)$$

$$\begin{cases} (\cos \bar{\beta} \cos \bar{\gamma} - \sin \bar{\alpha} \sin \bar{\beta} \sin \bar{\gamma})x_{c1} + (-\cos \bar{\alpha} \sin \bar{\gamma})y_{c1} + (\sin \bar{\beta} \cos \bar{\gamma} + \sin \bar{\alpha} \cos \bar{\beta} \sin \bar{\gamma})z_{c1} = \tilde{x}_{c1} \\ (\cos \bar{\beta} \sin \bar{\gamma} + \sin \bar{\alpha} \sin \bar{\beta} \cos \bar{\gamma})x_{c1} + (\cos \bar{\alpha} \cos \bar{\gamma})y_{c1} + (\sin \bar{\beta} \sin \bar{\gamma} - \sin \bar{\alpha} \cos \bar{\beta} \cos \bar{\gamma})z_{c1} = \tilde{y}_{c1} \end{cases} \quad (3c)$$

where  $\mathbf{R}(\bar{\alpha}, \bar{\beta}, \bar{\gamma})$  are rotation matrices. With Eqs. (3b) and (3c),  $\sin \bar{\gamma}$  and  $\cos \bar{\gamma}$  are calculated, and  $\bar{\gamma}$  is obtained.



(a)



(b)

**Fig. 14.** (a) Coordinate of ground SSPS verification system and (b) aerial structure and positions of Beidou sensors.  $OXYZ$  is the geodetic coordinate system,  $O_1X_1Y_1Z_1$ : the receiving antenna coordinate system;  $O_2X_2Y_2Z_2$ : the overall aerial structure coordinate system;  $O_3X_3Y_3Z_3$ : the transmitting antenna coordinate system; GPS: Global Positioning System; B1: Beidou sensor 1; B2: Beidou sensor 2; B3: Beidou sensor 3.

Until now, the lengths of the three cables have been adjusted to control the position and attitude of the aerial structure. The pointing direction of the condenser can be adjusted in real-time to track the sun. Nonlinear effects such as elasticity, thermal expansion, contraction of cables, and error of the windlass can be included in the control equation. These parameters can be determined through trial and error.

The beam direction of the transmitting antenna can be adjusted mechanically with the A/B axis or electronically with phase shifters.

## 6 Thermal control of photoelectric conversion and microwave conversion

Heat dissipation is a major issue in OMEGA SSPS. For the aerial structure, there are two heat sources: waste heat from the PV array and microwave power devices because the conversion efficiencies of the PV array and microwave power devices cannot reach 100%. Two steps are required to radiate waste heat from the PV array. First, utilizing a heat pipe, the waste heat of the top-shaped PV array can be utilized to heat the radiator efficiently. Second, waste heat radiates to outer space. The topology and layout of a thin cool plate embedded in a heat pipe should be optimized in the first step. Second, a high-efficiency heat radiator inspired by a butterfly wing was designed. The butterfly wing is lightweight and large.

The waste heat of the transmitting antenna is another issue that should be carefully addressed. Heat dissipation is an extremely challenging problem in sandwich-structured transmitting antennas. In the innovative design concept of OMEGA 2.0, the PV array, microwave power devices, and transmitting antenna are separated. Therefore, the heat dissipation problem could be reduced to some extent. However, considerable heat is produced during the DC-to-RF conversion process. If the waste heat is not efficiently dissipated, microwave power devices will deteriorate. Thus, a heat dissipation method was proposed, and its effectiveness was experimentally verified [25,26].

## 7 Rectenna optimization design

The rectenna receives and converts the incoming microwave power to DC power. The converted DC power was synthesized with rectenna circuits. In the experiment, a microstrip antenna with an air substrate was adopted as the receiving antenna element. The rectenna array is divided into three rings, as illustrated in Fig. 15. For the inner ring of the rectenna array marked in red, each receiving element was connected to a Schottky diode. Two and four receiving elements were connected to the diode for the two outer rings, marked in orange and yellow.

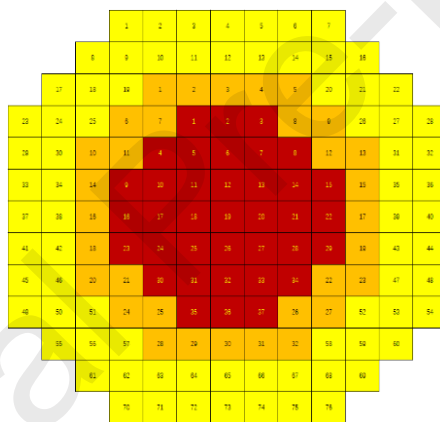


**Fig. 15.** Illustration of rectenna array.

The receiving element should have a high aperture efficiency to collect incoming microwave power efficiently. Simultaneously, the rectenna array should have the same polarization as the transmitting antenna. In this experiment, left-hand circular polarization-receiving elements/subarrays with an average aperture efficiency of 92.1% were adopted. The incident microwave power density, gain of each type of receiving element, voltage standing wave ratio (VSWR), axis ratio (AR), calculated half-power beamwidth (HPBW), and aperture efficiency (AE) are presented in Table 2

**Table 2**

Parameters of receiving elements.

Type	Gain ( dBi )	VSWR	AR ( dB )	HPBW (°)	AE
1-1	8.49–8.62	1.01–1.15	0.10–0.86	Elevation plane 68.54–70.21	93.98%–96.84%
				Azimuth plane 69.82–70.88	
2-1	11.58–11.72	1.02–1.21	0.10–1.20	Elevation plane 66.70–68.63	95.72%–98.86%
				Azimuth plane 32.20–33.16	
4-1	14.20–14.76	1.01–1.29	0.10–1.60	Elevation plane 31.45–33.38	87.50%–99.54%
				Azimuth plane 31.83–34.72	

The impedance of the rectenna element should match that of the rectifier circuit. In addition, the incident microwave power affects the RF–DC conversion efficiency of the rectifier. Through extensive simulations and experiments, it was found that when the incident microwave power is within 22 dBm, the RF–DC conversion efficiency exceeded 50%. In contrast, when the incident microwave power was between 22 and 27 dBm, the RF–DC conversion efficiency exceeded 60%. Finally, a double-voltage rectifier circuit was employed, and an average RF–DC conversion efficiency of 59.4% was achieved. For DC power synthesis, the circuit topologies are optimized for rectifiers with different output voltages and currents. It must be stressed that isolation circuits must be added to prevent inrush currents from breaking down the rectifier diodes. The DC power synthesis efficiency of the rectenna array is 74.1%.

## 8 Microwave beam pointing accuracy measurement

Apart from the measurement of the position and attitude of the aerial structure, shell temperature of microwave power devices, mechanical accuracy, ambient temperature, and wind load, the incident microwave power density on the rectenna plane and the axis ratio of the transmitting antenna were measured to meet the requirements of beam-pointing accuracy.

Monitoring antennas were utilized to obtain the incident microwave power-density distribution on the rectenna. Each monitoring antenna element was connected to a microwave power sensor, and the monitoring antenna elements were located symmetrically. When two symmetrical microwave power sensors have different readings, it means that there is a beam-pointing error. The beam-pointing error information is then fed back to the transmitting antenna. With phase shifters, the beam-pointing error can be compensated. Another point to note is that mechanical adjustments should accompany electronic adjustments.

Furthermore, 13 linear polarization monitoring antennas were employed to measure the axis ratio of the transmitting antenna (Fig. 16), and each monitoring antenna was connected to a stepping motor to record the received microwave power. The axis ratio of the transmitting antenna was calculated by subtracting the maximum received power from the minimum received power.

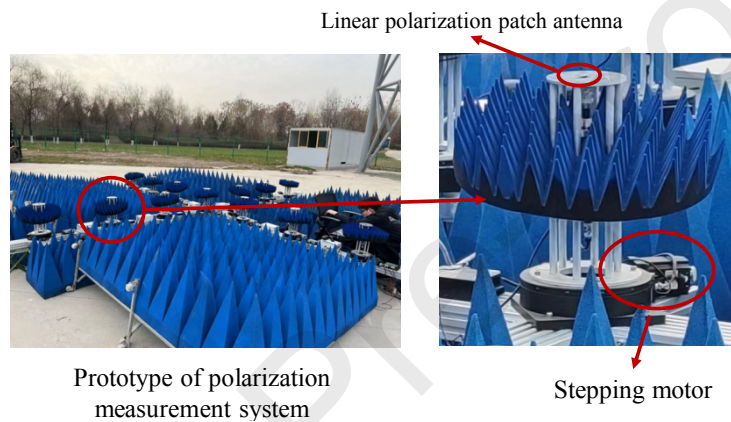


**Fig. 16.** Microwave beam polarization measurement equipment.

## 9 Smart structure design and development

To meet the system requirements of high precision, smartness, and light weight, multidisciplinary, systematic, and smart design ideas based on electromechanical coupling theory are employed in the design process, including structural type, topology, shape, and size optimization. Optimization methods were adopted in the aerial triangle backup-frame structure design, condenser backup-frame structure design, condenser mirror design, and top-shaped PV array support structure, and so on (Fig.17).



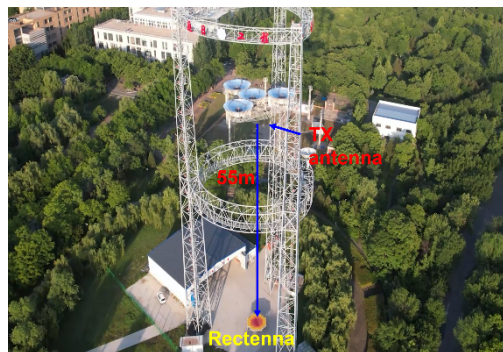
**Fig.17.** Prototype of condenser and support truss structure.

The mechanical transmission mechanism optimization designs include the transmitting antenna A/B axis and support frame, large-span flexible cable drive and high-precision pulley block structure, servo and hoist, support, and motor system of the overall aerial structure.

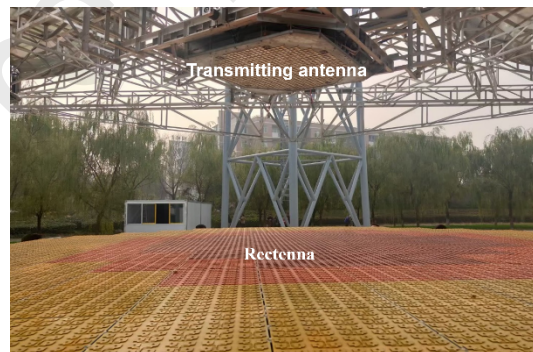
Electromechanically integrated structural designs include air substrate microstrip patch transmitting and receiving elements, photoelectric conversion, and microwave conversion systems.

## 10 Development and experiment of ground verification system

The SSPS ground verification system presented in Fig. 18 was successfully developed based on in-depth theoretical research and technical breakthroughs. It included spherical crown condensers and photoelectric conversion systems, transmitting and receiving antennas, smart aerial support structures, support towers, large-span cable driving mechanisms, and measurement and control systems.



(a)



(b)



(c)

**Fig. 18.** (a) Prototype of ground SSPS verification system; (b) prototype of transmitting antenna and rectenna; (c) prototype of ground SSPS verification system (upward view).

The prototype of the transmitting antenna presented in Fig. 19 has an aperture size of 1.2 m; it has a 5.8 GHz crystal oscillator with a stability of  $10^{-8}$ , a pre-stage power amplifier, a 1-to-176 power divider with equal amplitude and phase output, 176 final-stage power amplifier modules, and a heat sink. Each power amplifier module has a power amplifier, phase shifter, and power supply. The transmitting antenna has 704 air-substrate microstrip patch elements, and the transmitting antenna has a DC–RF efficiency of 42.55%.

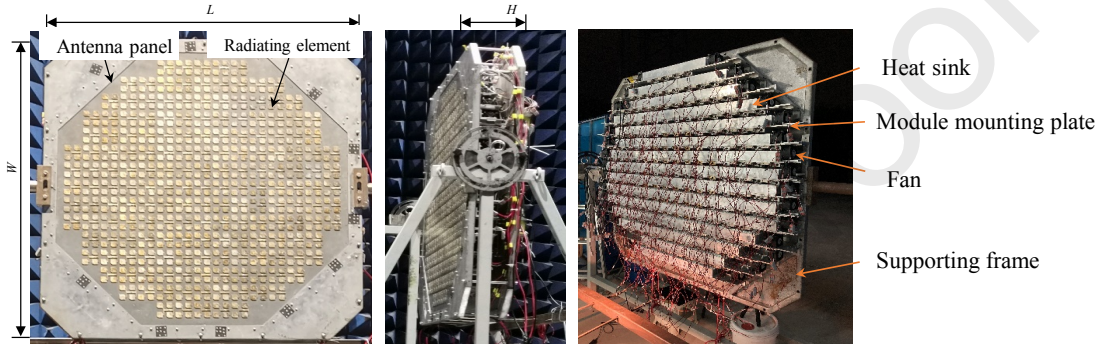


**Fig.19.** Prototype of transmitting antenna.  $L$ : length;  $W$ : width;  $H$ : height.

The rectenna array has an aperture size of 5.2 m, as illustrated in Fig. 20. Each receiving element is an air-substrate microstrip patch-receiving antenna. The rectenna array comprises 14500 receiving elements and 7200 Schottky rectifier diodes.

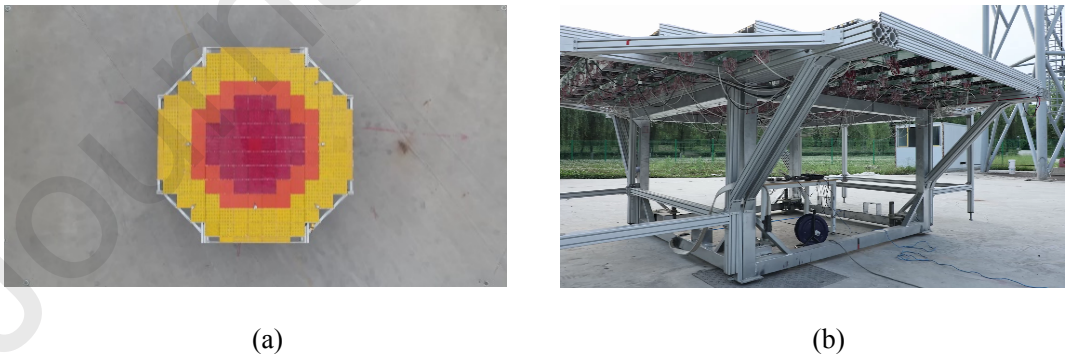


**Fig. 20.** (a) Front view of rectenna array, and (b) side view of rectenna array.

Fig. 21(a) presents the measurement, control, and power-supply computers in the main control room. The visual menu supported the selection of various test parameters. It can also display the microwave beam-pointing accuracy, incident microwave power density on the rectenna array, attitude angles of the condensers, temperature distributions of the PV array and power amplifiers, ambient temperature, wind speed,

and direction of the environment in real time. Fig. 21(b) illustrates a prototype of the condenser and attitude and control windlass. The lengths of the three cables were calculated and adjusted with three windlasses to guarantee that the position and attitude of the four condensers were within an allowable range, such that the electrical performance of the transmitting antenna could be guaranteed.



**Fig. 21.** (a) Measurement, control, and power supply computers in control room, and (b) condenser and attitude and control windlass.

Located on the campus of Xidian University, the Sun Chasing Project is a ground demonstration and verification system for MWPT-based SSPS that can support a variety of experiments and the experimental verification of innovative design and manufacturing technologies. Various experimental studies have been conducted based on this experimental system, and a large amount of experimental data has been accumulated. The experimental results of MWPT at 5.8 GHz are summarized in Table 3 [15-17, 25]. The table also presents the results of the MWPT experiments in Hyogo Prefecture, Japan, in 2015 and 2019, and Hawaii, USA, in 2008.

**Table 3**

Experimental results of China, Japan, and the United States.

Location		Transmission distance	Transmitted power (W)	BCE (%)	DC-DC (%)
China [25]	Xi'an	(2022) 55 m	2081	87.3	15.05

Japan	Hyogo	(2015)	55 m	1800	66.00	9.88
[16]						
UAV		(2019)	10/30 m	1600	—	Received power
[17]						60/42 W
USA	Hawaii,	(2008)	148 km	20	—	—
[15]						

UAV: unmanned aerial vehicle.

The experiment conducted by Xidian University in June 2022 has significant advantages in some key technical indices. In addition, the SSPS ground verification system can mimic the key links of a real SSPS in outer space, such as sun tracking, photoelectric conversion, high voltage and huge power transmission and management, and smart mechanical structures, which are not yet available in Japanese or American experiments.

The developed SSPS ground verification system comprises several subsystems, including solar energy collection and conversion, DC power transmission and management, transmitting antenna, and rectenna subsystems. The efficiency of each subsystem was measured during the experiment, and the results are summarized in Fig. 22. The total efficiency was 1.15%, with a DC–DC wireless power transmission efficiency of 15.05%. Fig. 22 demonstrates that the total transmission efficiency is restricted by solar energy collection and conversion efficiencies. This is because a cheap and low-efficiency silicon PV array was utilized (~18%) owing to funding limitations. The measured DC output power of the verification system was approximately 736 W.

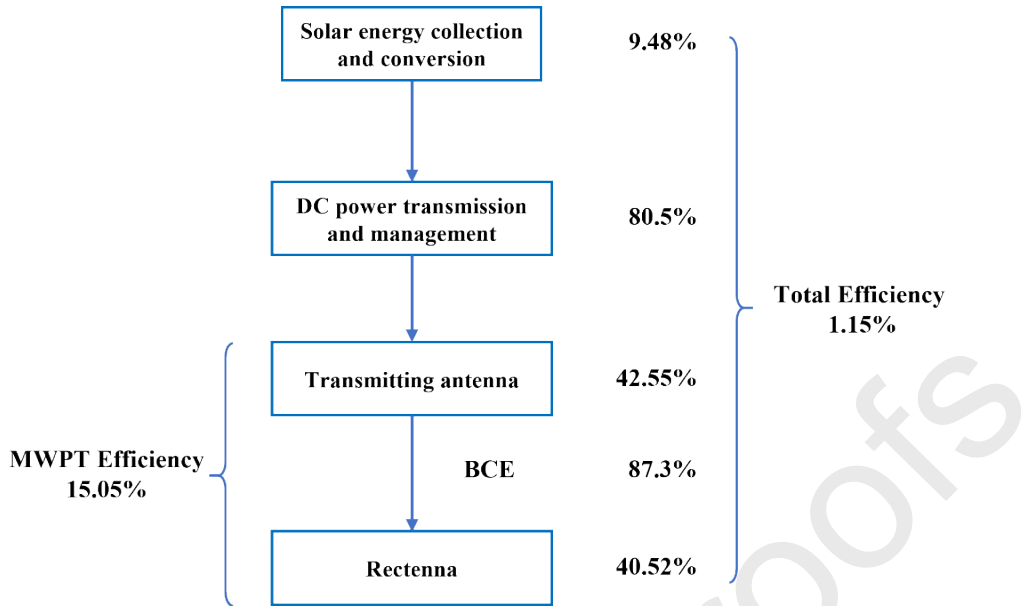


**Fig. 22.** Efficiencies of full links of ground verification system

## 11 Concluding remarks

Valuable experience is gained through theoretical analysis, simulation, system development, and extensive experiments, which can be summarized as follows.

1. Based on the innovative design of OMEGA 2.0, a multiphysics and multidisciplinary coupling theoretical model was established, and a systematic optimization design method was proposed, which laid the theoretical foundation for the theoretical analysis, numerical simulation, and development of an SSPS ground verification system.
2. The world's first full-link and full-system space solar power satellite ground demonstration verification system has been developed and has the capacity for sun tracking, photoelectric conversion, high-voltage and huge power transmission and management, microwave conversion and emission, microwave wireless power transmission, and microwave reception and rectification. The system lays a solid foundation for the innovation of the MWPT-based SSPS.
3. A high BCE of 87.3% and a total DC–DC efficiency of 15.05% were achieved for the developed MWPT system working at 5.8 GHz. The transmitting antenna and rectenna were separated by 55 m, and the transmitted power was 2081 W. This result is better than the world's latest experimental results in Hyogo Prefecture, Japan (BCE of 66% and DC–DC efficiency of 9.88% were obtained for a system with the same working frequency and transmission distance, and the transmitted power was 1800 W).
4. As the next step, the necessary research activities should be conducted via more in-depth experiments and innovative research based on a verification system.
5. Some improvements can be made to enhance the system's efficiency. For example, in a Sun Chasing Project, a cheap and low-efficiency silicon PV array was utilized

because of funding limitations. In the future, a high-efficiency GaAs PV array could be adopted. In addition, high-efficiency power amplifiers should be specially developed for MWPT applications where there is no working bandwidth requirement. In addition, employing AiP (antenna in package) technology, the power amplifier, phase shifter, power supply module, and antenna element/subarray can be integrated to reduce the size and loss of the transmitting antenna.

6. Note that the size, transmitted power level, and environment on Earth are quite different from those in outer space; therefore, a similarity analysis of the ground verification system and a real SSPS in outer space should be performed. Based on the similarity theory, the experience gained and the technologies developed could be beneficial for constructing a real SSPS.

7. In the future, we will focus on the utilization of a transmitting antenna to feed multiple moving targets. Real-time target detection and accurate beam-control technologies should be developed in this case.

## Acknowledgments

The development of the ground OMEGA 2.0-based SSPS verification system was supported and assisted by Jin Huang, Wei Liang, Feng Zheng, Liwei Song, Xianli Li, Na Li, Sihao Qian, Shunxi Lou, Chaoliu Ge, Guanheng Fan, and the PhD and MSc students in our research group. The authors express their special thanks for their support and assistance.

## Compliance with ethics guidelines

Baoyan Duan, Yiqun Zhang, Guangda Chen, Ze Zhao, Jianwei Mi, Xun Li, Lin Yang, and Xi Li declare that they have no conflict of interest or financial conflicts to disclose.

## References

- [1] Statistical review of world energy. Report. London: BP; 2020
- [2] Glaser PE. Power from the sun: its future. *Science* 1968;162(3856):857–61.
- [3] Mankins JC. New directions for space solar power. *Acta Astronaut* 2009;65(1–2):146–56.
- [4] Seboldt W, Klimke M, Leipold M, Hanowski N. European sail tower SPS concept. *Acta Astronaut* 2001;48(5–12):785–92.
- [5] Sasaki S, Tanaka K, Higuchi K, Okuzumi N, Kawasaki S, Shinohara N, et al. A new concept of solar power satellite: Tethered-SPS. *Acta Astronaut* 2007;60(3):153–65.

- [6] Hou X, Wang L, Zhang X, Zhou L. Concept design on multi-rotary joints SPS. *J Astronaut* 2015;36(11):1332–8. Chinese.
- [7] Carrington C, Fikes J, Gerry M, Perkinson D, Feingold H, Olds J. The Abacus/Reflector and integrated symmetrical concentrator: concepts for space solar power collection and transmission. In: Proceedings of the 35th Intersociety Energy Conversion Engineering Conference and Exhibit; 2000 Jul 24–28; Las Vegas, NV, USA; 2000.
- [8] Mankins J. SPS-ALPHA: the first practical solar power satellite via arbitrarily large phased array. In: Proceedings of the 10th International Energy Conversion Engineering Conference; 2012 Jul 30–Aug 1; Atlanta, GA, USA; 2012.
- [9] Jaffe P, Pasour J, Gonzalez M, Spencer S. Sandwich module development for space solar power. In: Proceedings of the 28th International Symposium on Space Technology and Science; 2011 Jun 5–12; Okinawa Prefecture, Japan; 2011.
- [10] Duan B. [A novel design project of space solar power station (SSPS) called OMEGA project]. In: The 2nd Symposium of Space Information Technology and Application of Chinese Academy of Engineering; 2014 Sep 21–23; Xi'an, China; 2014. Chinese.
- [11] Yang Y, Duan B, Huang J, Li X, Zhang Y, Fan J. SSPS–OMEGA: a new concentrator system for SSPS. *Chin Space Sci Technol* 2014;34(5):18–23. Chinese.
- [12] Yang Y, Zhang Y, Duan B, Wang D, Li X. A novel design project for space solar power station (SSPS–OMEGA). *Acta Astronaut* 2016;121:51–8.
- [13] Cash I. CASSIOPeIA solar power satellite. In: Proceedings of 2017 IEEE International Conference on Wireless for Space and Extreme Environments (WiSEE); 2017 Oct 10–12; Montreal, QC, Canada; 2017.
- [14] Arya M, Lee N, Pellegrino S. Ultralight structures for space solar power satellites. In: Proceedings of The 3rd AIAA Space Structures Conference, Spacecraft Solar Array Structures I; 2016 Jan 4–6; San Diego, CA, USA; 2016.
- [15] Kaya N, Iwashita M, Little F, Marzwell N, Mankins JC. Microwave power beaming test in Hawaii. In: Proceedings of the 60th International Astronautic Congress; 2009 Oct 12–16; Daejong, Republic of Korea; 2009.
- [16] Mihara S, Sato M, Nakamura S, Sasaki K, Homma Y, Sasaki T, et al. The result of ground experiment of microwave wireless power transmission. In: Proceedings of the 66th International Astronautic Congress; 2015 Oct 12–16; Jerusalem, Israel; 2015.
- [17] Shinohara N, Hasegawa N, Kojima S, Takabayashi N. New beam forming technology for narrow beam microwave power transfer. In: Proceedings of the 8th Asia-Pacific Conference on Antennas and Propagation; 2019 Aug 4–7; Incheon, Republic of Korea; 2019.
- [18] Rodenbeck CT, Jaffe PI, Strassner II BH, Hausgen PE, McSpadden JO, et al. Microwave and millimeter wave power beaming. *IEEE J Microw* 2021, 1(1): 229–59.

- [19] Vedda JA, Jones KL. Space-based solar power: a near term investment decision. El Segundo: Center for Space Policy and Strategy; 2021.
- [20] Liu C, Li K, Huang K. [Development of microwave power transmission study]. J Kunming Univ Sci Technol 2011; 36(sup):19–22. Chinese.
- [21] Duan B. Fundamental, technology and prototype experiment of MWPT & SSPS in China. In: IEEE Wireless Power Transfer School; 2021 May 27–Jun 2, San Diego, CA, USA; 2021.
- [22] Duan BY. [The improved OMEGA project of SSPS with MWPT and omnidirectional scanning antenna]. Sci Sin Tech 2023;53(1):139–44. Chinese.
- [23] Duan BY. [The main aspects of the theory and key technologies about space solar power satellite]. Sci Sin Tech 2018;48(11):1207–18. Chinese.
- [24] Li X, Duan B, Song L, Zhang Y, Xu W. Study of stepped amplitude distribution taper for microwave power transmission for SSPS. IEEE Trans Antennas Propag 2017;65(10):5396–405.
- [25] Duan B, Zhang Y, Chen G, et al. Report of Chasing the Sun Project. Xi'an: Xidian University; 2022.
- [26] Fan G, Duan B. Topology and bionic-based thermal design of space solar power station and the application in SSPS—OMEGA. Chin J Comput Mech 2021;38(4):445–51.
- [27] Qian S, Duan B, Lou S, Ge C, Wang W. Investigation of the performance of antenna array for microwave wireless power transmission considering the thermal effect. IEEE Antennas Wirel Propag Lett 2022;21(3):590–4.

The authors declare that they have no known competing financial interests or personal relationships that could have appeared to influence the work reported in this paper.